Experimental and numerical study on the plane-strain blanking process on an AHSS sheet

Citation: Wang, Kai, and Tomasz Wierzbicki. "Experimental and Numerical Study on the Plane-Strain Blanking Process on an AHSS Sheet." International Journal of Fracture 194, no. 1 (July 2015): 19–36.

As Published: http://dx.doi.org/10.1007/s10704-015-0034-1

Publisher: Springer Netherlands

Persistent URL: http://hdl.handle.net/1721.1/103310

Version: Author's final manuscript: final author's manuscript post peer review, without publisher's formatting or copy editing

International Journal of Fracture manuscript No.
(will be inserted by the editor)

Experimental and Numerical Study on the Plane-strain Blanking Process on an AHSS Sheet

Kai Wang · Tomasz Wierzbicki

Received: date / Accepted: date

Abstract The blanking/trimming/cropping process introduces a substantial plastic deformation to the sheet metal and causes premature edge fracture during the subsequent forming process. In an attempt to understand how the blanking process affects edge fracture, an experimental and numerical study was undertaken on the plane-strain blanking process. Blanking tests on a DP780 steel sheet were carried out on a special fixture utilizing a in-situ microscope for the Digital Image Correlation (DIC) deformation measurement. The DIC method provides a detailed deformation field of the specimen that has not been reported in any other publications before. Interrupted tests were carried out to study the crack formation and propagation during the blanking procedure, while Scanning Electron Microscope (SEM) was applied to examine the blanked surface quality as well as the edge profile after test. Following the experimental study, a detailed Finite Element Model with mesh size of 0.01mm in the critical region was established for the numerical investigation. The model features (a) a non-associated Hill 48 flow rule, (b) von-Mises Yield condition and (c) modified Mohr-Coulomb (MMC) fracture model. With material parameters calibrated from the in-plane tests as well as accurate boundary conditions measured in actual tests, the Finite Element model accurately predicted the blanking process quantitatively. The current study also gave quantitative values of the parameters of interest during the blanking test, such as the global load displacement response and the local strain gradient history. The geometrical features of the blanked edge, i.e. the amount of roll over, the extent of the burnished zone and fracture zone were all accurately predicted by the present simulation.

Keywords Blanking test · DIC measurement · Finite Element simulation · Edge fracture · Dual Phase steel

Kai Wang (✉) · Tomasz Wierzbicki
Impact and Crashworthiness Laboratory, Department of Mechanical Engineering, Massachusetts Institute of Technology, Cambridge, MA 02139, USA
E-mail: wangkai@mit.edu

Highlights

1. The whole deformation field of the specimen during a blanking process was measured by DIC method with high resolution using an in-situ microscope.
2. The numerical simulation of the blanking process correlates well with the test results with mesh size of 0.01mm in the critical region using accurate boundary conditions measured from tests.
3. The out-of-plane fracture behavior of the DP780 sheet during blanking process was accurately predicted by FE model using material parameters calibrated for the in-plane direction.

1 Introduction

Due to the high efficiency and easy quality control, the sheet blanking/trimming/hole piercing is used widely in a mass production environment, Figure 1a. Products from a small door hinge to big vehicles and trains, their manufacturing processes all involve the sheet blanking operation. However, blanking also introduces a substantial plastic deformation in the local vicinity of the edge, as illustrated in Figure 1b(Li, 2000b). The blanking process reduces material ductility in the subsequent

forming operation and cause the premature edge fracture (Shih et al, 2010). According to the experimental study by Wang et al (2014), the fracture limit of a blanked specimen was greatly reduced, as compared with milled specimen or water-jet cut specimen which can be taken as crack-free material (Dykeman et al, 2011). The same finding was also reported by many other authors (Konieczny and Henderson, 2007; Golovashchenko and Ilinich, 2005; Golovashchenko, 2008). The issue of edge fracture poses a great challenge to the forming community with the dramatical growth of the application of light-weight materials such as aluminum alloys and Advanced High Strength Steels (AHSS). Traditional FE models are not capable of predicting the edge fracture. An appropriate inclusion of the effects caused blanking process is the corner stone in edge fracture modeling Wang et al (under review). In order to do that, an accurate experimental and numerical study on the sheet blanking process is required.

Sheet blanking process has been studied extensively in the open literature using mostly experimental methods. Understanding blanking conditions and the resulted edge quality is necessary to optimize the blanking procedure. The most important blanking conditions include tool gap, tool sharpness and cutting angle (Li, 2000a). Geometrical features of the blanked edge, illustrated in Figure 1a, greatly depend on these conditions. On the experimental side, Samuel (1998) performed the hole piercing process with different combinations of (a) two die clearances, (b) two types of die/punch sharpnesses and (c) two different sheet materials (cold rolled steel and annealed steel). In general, larger die clearance and duller punch/die result in higher blanking force and larger punch displacement (penetration) before total rupture. Li (2000a) performed a comprehensive study on blanking aluminum alloy sheets and studied the formation of burr, which is an important quality benchmark of a blanked edge and may cause severe damage on the workpiece during the forming process. In that study, different tool sharpnesses, die clearances and cutting angles were tested. It was found that sharper cutting tool, smaller die clearance and a moderate cutting angle could avoid the generation of burrs. Golovashchenko (2006) investigated the mechanism of burr generation on a different material which is Advanced High Strength Steel (AHSS). A methodology named "robust trimming technique" was proposed by them which utilizes a sharp die, a dull punch head and an elastic offal holding pad to ensure the crack initiates from the sharp die side which relocates the burr from the work part into the offal part. However, in all those studies the experiments were carried out in such a way that the specimens were checked only before and after the test, while what happened to the specimens during the blanking process was not available. A pioneering study by Goijaerts et al (2000) recorded a series of images on the specimen during a plane-strain blanking process and made use of the Digital Image Correlation (DIC) method to extract strains from those images during the post-processing. However, considering the blanking process introduces a severe localization with a high gradient in a small tool gap, those images reported have a limited spatial resolution. At the same time, the study made use of the natural contrast information of the material, which will vary drastically during the test due to the large deformation. In addition, the natural contrast of metals is also highly sensitive to the light source, which causes additional system error to the measurement.

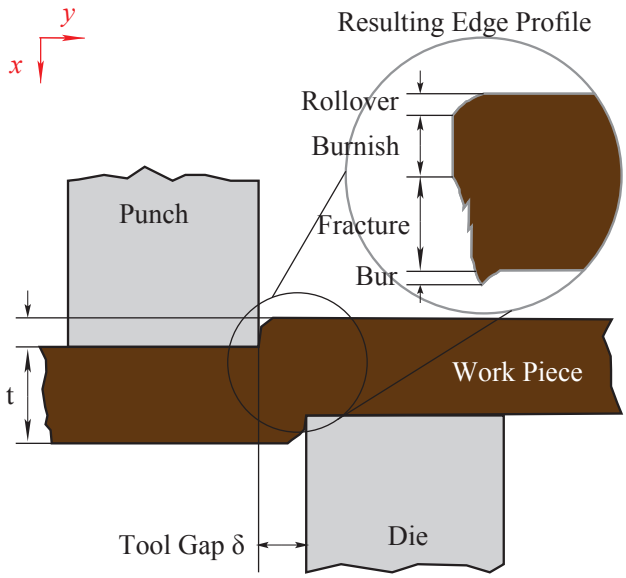

(a)

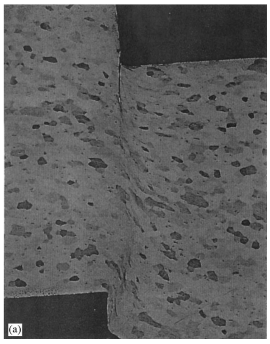

(b)

Fig. 1: (a) Schematics of the blanking process, (b)a typical blanked-edge profile(Li, 2000b).

Recent research shows the sheet blanking process tends to cause a premature edge fracture during the

subsequent forming process. Hole expansion test results indicate that a blanked edge usually possesses a much lower stretch limit compared with milled edge(Konieczny and Henderson, 2007; Wang et al, 2014). An attempt to understand why the blanked edge has lower fracture limit and how to model it was reported by Dalloz et al (2009) where micro-structure observation was carried out and pre-damage in the form of micro voids was observed at the blanked edge.

Due to the high geometrical nonlinearity and material nonlinearity, it is too complex to analyze the blanking process analytically(Zhou and Wierzbicki, 1996). Instead, the numerical way is often chosen for detail analysis in comparison with experiments. However, it is very challenging to perform an accurate FE simulation on the blanking process in view of the high strain gradient in the shear affected zone and the enormous distortion in materials there. There is lack of reliable experimental data about the local deformation and strain gradient in this area. In an early work by Samuel (1998), the author employed a 2D axisymmetric model to perform blanking simulation. However, the FE mesh did not have enough spatial resolution to capture the high strain gradient from today's point of view. The analysis mainly presented a qualitative correlation between tests and simulation while a more precise quantitatively comparison was not available. A quantitative comparison between tests and FE simulation was reported in Goijaerts et al (2000). The study obtained a good correlation in the load displacement response measured from experiments and the simulation. It also predicted the logarithmic strain fields with good accuracy measured by DIC from tests. More advanced numerical techniques have been proposed recently in blanking simulation. Thipprakmas et al (2008) made use of adaptive re-meshing as well as Arbitrary Lagrangian-Eulerian (ALE) method in an effort to address the high strain localization and material rotation during FE simulation of the blanking process of a S45C mild steel. Geometrical defects on the blanked surface were accurately predicted. With the advancement in computational power, much finer FE models cam be developed in blanking simulation. A recent work by Hu et al (2014) used a 2D plane strain model with very fine mesh of order of 0.01mm and accurately predicted the blanked edge profile of aluminum alloys. The burr heights were accurately predicted quantitatively. An appropriate fracture model is also critical for blanking simulation. Hambli and Reszka (2002) compared 10 different fracture models for blanking fracture prediction including Rice and Tracy model (1969) and Cockroft and Latham model (1966). However the fracture models were calibrated using the blanking test itself therefore lost most of generality. Also the simulated load displacement response was much higher than that measured from tests. Hu et al (2014) obtained good prediction results using the strain-based damage accumulation model with the Rice and Tracey (1969) expression of fracture locus.

Despite all of the above fine studies, one common missing part is the quantitative measurement of the local deformation and strain gradient in the blanked zone, which is important to verify if the FE element simulation correlates with the test. Most experimental studies on the blanking process follows a strategy of first performing the blanking and then carrying out inspection and measurement on the blanked edge after test. Also the blanking load displacement curve was rarely reported. In fact, it is difficult to perform such measurements during the blanking test. As for load displacement response, because the blanking test device usually had a complicated alignment system to ensure the accuracy of die clearance during the test, such as the case of Thipprakmas et al (2008), the load information measured by test machines was a combination of friction force within the tools, alignment spring reaction force and the blanking force. It would require a great effort to distinguish the net blanking force from the measured data. In terms of blanking strain measurement, during hole piercing process the blanked zone is inside the specimen and is not observable to measuring equipments like cameras. By contrast, in plane-strain blanking process, the deformation can be measured from the side surface by a camera. However, the small blanking area as well as high strain gradients poses a great challenge to the measurement accuracy. Stegeman et al (1999) tried to record the history of the plane-strain blanking process using a camera. But the images do not have enough spatial resolution within the tool gap. Also, methods such as Digital Image Correlation were not capable of measuring the whole-field deformation with enough accuracy.

There are two main objectives of the present paper. First, to perform an experimental study that could provide an accurate measurements of the specimen deformation as well as the blanking force displacement response, in addition to the usually measured blanked profile geometries after tests. Second, to develop a Finite Element tool that could predict the blanking process with good correlation with the test results in terms of global load displacement response, local strain gradient history, the blanked edge profile and so on. To that end, a novel plane-strain blanking apparatus was designed and a comprehensive blanking test program was carried out on a DP780 steel sheet with thickness of 1.6mm and reported Section 2. During the test, a mi-

croscope was introduced to perform Digital Image Correlation (DIC) deformation measurement in real time on the side surface of the specimen within the small tool gap. The tests provided quantitative details that help guide the Finite Element simulation afterwards. After the tests, a 2D plane-strain Finite Element model was developed in Section 4 to simulate the blanking process. Material parameters were obtained from a general calibration program consisting of multiple in-plane tests as reported in an earlier publication by the authors (Wang et al, 2014). The study revealed that a simplified boundary condition assuming the tooling system to be ideally rigid, which was the case in most open literature (Thipprakmas et al, 2008; Hu et al, 2014), did not give good agreement with the test results. Boundary conditions as measured from the tests, including deformable blanking tool, die clearance variation and mis-alignment in the tool were then modified and the resulting FEA model yielded an accurate prediction.

2 Test program

2.1 Apparatus design and test setup

In a blanking test on AHSS sheet, big challenges comes from the very small gauge section (around 2×2mm) as well as the high blanking load associated with this test. The tool gap between the punch head and the die defined in Figure 1a is only of the order of 0.1mm. However, the force required to blanking the AHSS sheet is of order of 10kN which can cause substantial deformation in the tools. In view of this, elastic deformation of the blanking tools is not negligible during the test and a high system rigidity is required. In the current study, the punch head as well as the die was designed to be a single block as illustrated in Figure 2a. There was no moving part within each piece to maximize the tool rigidity. Different die clearances of interest were obtained by using dies of different size. Both the punch head and the die were fabricated with A2 tool steel and heat-treated to a hardness of 62HRC, which corresponds to a yield strength of about 2200MPa. During the test, the punch head was connected directly to the upper cross head of the test machine while the die was connected to a test table (Figure 2a) which was fixed on the test machine's lower platform. The conical shape shoulder on the punch head was designed to help align the tool and ensure that the punch head and the die shares the same middle plane.

The specimen tested has a simple rectangular geometry and was illustrated in Figure 2b. It was fixed to the die by two die holders and tightened through four M3 screws. Three different die clearances δ/t as denoted in Fig. 1a in were tested which were 5%, 20% and 40%. The tests were performed on a screw drive 200kN MTS universal test machine at a cross-head speed of 0.01mm/min.

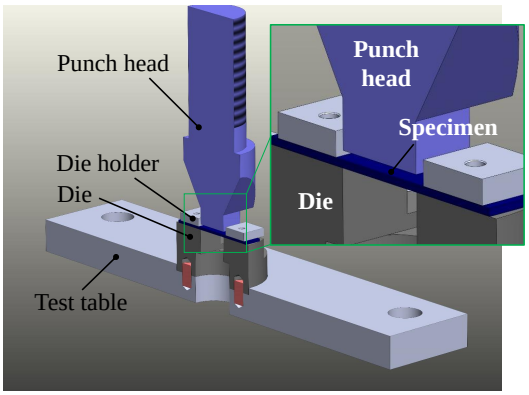

(a)

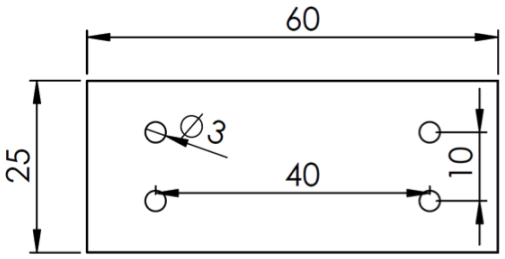

(b)

Fig. 2: (a) Illustration of the plane-strain blanking tools. (b) drawing of the tested specimen.

2.2 Blanking deformation measurement

Deformation of the specimen was recorded by a camera and processed through Digital Image Correlation (DIC) method in current study. To measure the deformation, the blanking apparatus need to be designed in such a way that the specimen can be observed by a camera and at the same time the tools will not block the view during the test. Since the tool gap is very small, the specimen can easily be blocked during the test when punch head moves forward. To avoid this, the specimen should not stay inside the tools. Instead, the blanking tools (die and punch head) need to have the same width as the specimen and their side surfaces should be aligned during the test. In addition, to measure the deformation in the very small tool gap with enough resolution, a high magnification ratio is needed. In current study, a

microscope was introduced to tackle to problem. The resulting pixel size is about 2.6μm. The test apparatus setup as well as the microscope arrangement was shown in Figure 3.

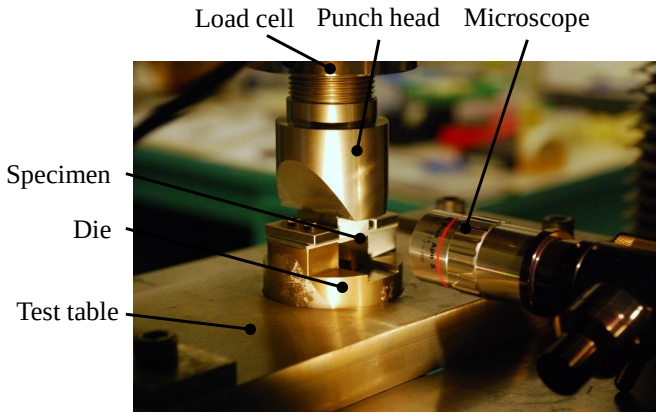

Fig. 3: Test setup and DIC deformation measurement using an in-situ microscope.

To use DIC method for deformation measurement, a random speckle pattern need to be applied before test on the specimen surface. Speckle pattern created by the commonly used spray can does not have enough resolution for the blanking test. A typical speckle pattern prepared by a spray can is shown in Figure 4a. The figure shows the side surface of the sheet specimen which has a thickness of 1.6mm. The speckles have a size of order of 0.2mm. There are only about 10 speckles in the thickness direction, while only 3 speckles in the tool gap in horizontal direction (as marked by vertical yellow solid line in Figure 4a). In the current study, an air brush with fluid ink was used to create a much finer speckle pattern as illustrated in 4b. The speckles generated this way have an average diameter of order of 0.02mm and provide enough spatial resolution for the current study.

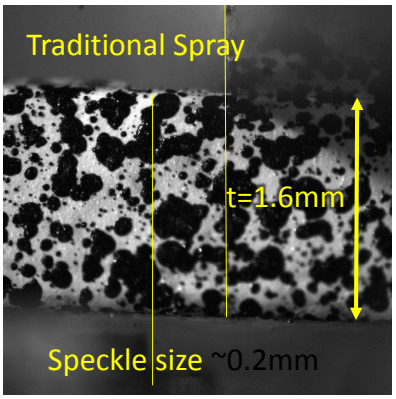

(a)

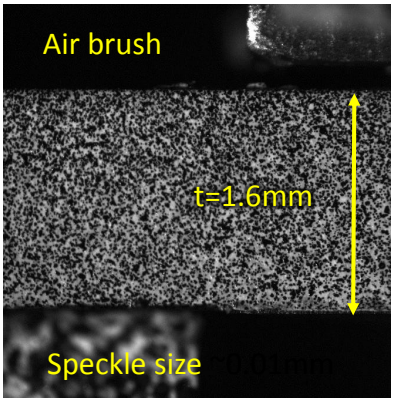

(b)

Fig. 4: Speckle patter created by (a) spray can and (b) air brush under microscope observation.

3 Test results

3.1 Sheet blanking sequence

A typical blanking sequence recorded by the microscope is shown in Figure 5, with Figure 5c denoting the image captured right before total separation, while Figure 5d correspond to the frame after total separation. In the images, punch head moved from left side right to blanking the specimen. The contour showed the logarithmic shear strain ε_{xy} calculated by DIC. During the post-processing, a subset size of 41 $\times$ 41 pixels was used while the subset step size chosen was 5 pixels. It is revealed that when the punch head moved forward, the specimen starts to deform and the deformation mainly concentrated around the tool gap. Severe strain localization happened before the total separation in the specimen. An abrupt fracture was observed. The crack initiation and propagation process happened so fast in the test that the camera did not capture it. DIC method failed to correlate the last image with good precision due to the sudden jump of the split part of the specimen after abrupt fracture. According to the DIC measurement, the deformation concentrates mainly inside the tool gap and decreased rapidly away from it. The localization becomes more obvious and the strain gradient increases when the punch head moves forward. Inside the tool gap and before total separation, there is a narrow region of material with high shear strain and that region roughly followed the path between the tool tip (Figure 5c).

Spatial distribution of three out-of-plane strain components before crack formation is presented in Figure 6. As expected, the major deformation is shear with max-

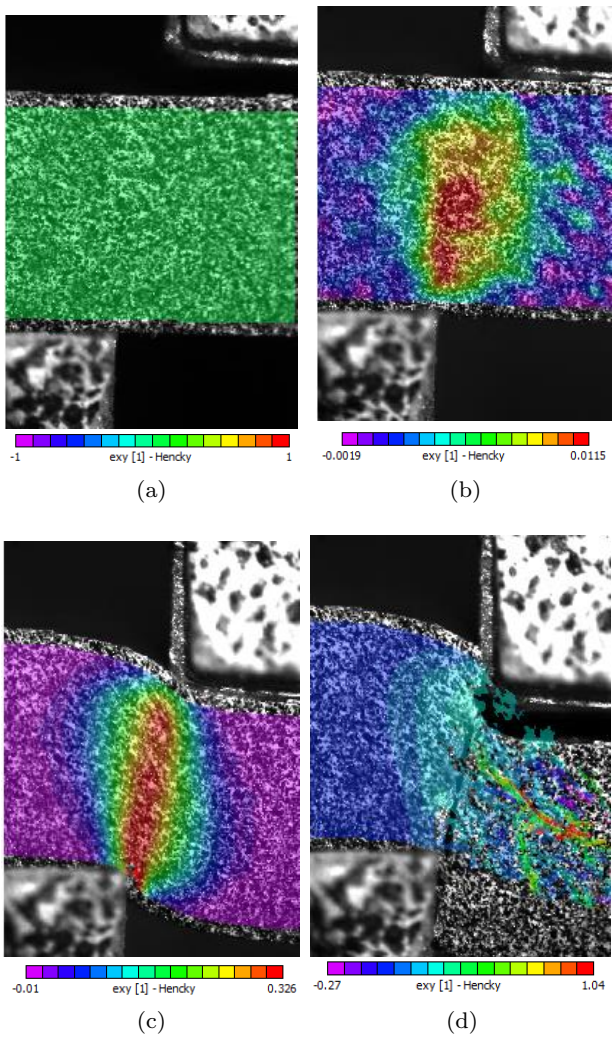

Fig. 5: Blanking test sequence measured by DIC, color code of the contour is ε_{xy}, $CL = 20\%$.

imum strain of 0.29. In addition, a substantial in-plane tensile strain component ε_{yy} developed close to the tool tips with a maximum value of about 0.15, in Figure 6c. Material in this region undergoes a combined loading of shear and tension. In the middle of the thickness direction, tensile strain component is almost zero and the loading condition there is shear dominated. Compressive strain component ε_{xx} in the thickness direction is smaller than the other two components with a maximum value of about 0.10. It concentrates inside tool gap and has a slight localization close to the tool tips. Note that there is a high strain gradient within the tool gap as can be observed in Fig. 5. The measured strains are expected to increase when further increasing the spatial resolution of images acquired by the microscope, and when reducing the step size during the DIC post processing. In view of this, it is important to have a consistent mesh size/step size between the tests and the numerical simulation in the following study.

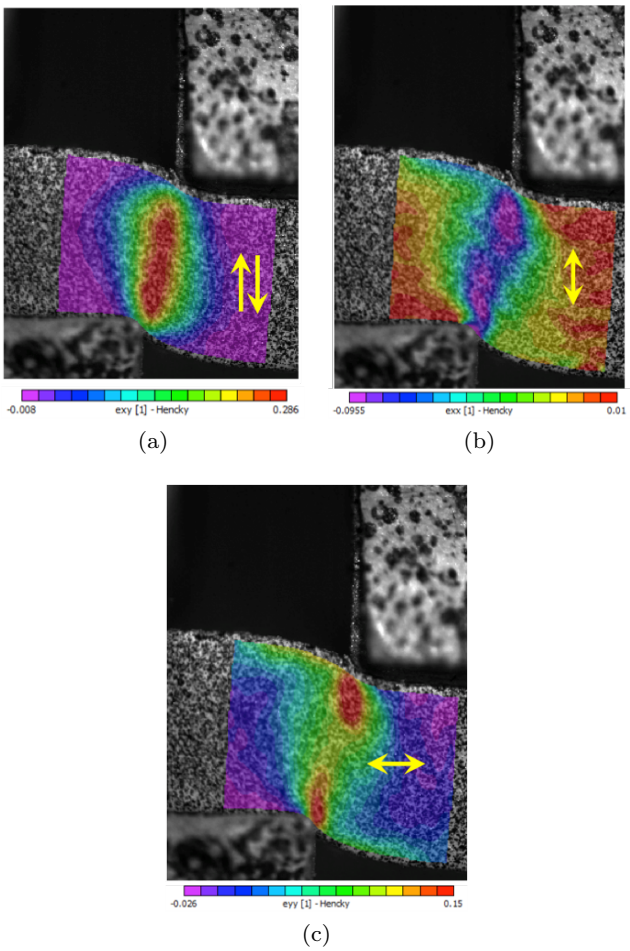

Fig. 6: Different strain components right before crack formation measured by DIC, (a) ε_{xy}, (a) ε_{xx}, (a) ε_{yy}.

3.2 Load displacement response and local extensometer history

The punch head was connected directly to the load cell on the cross head, as illustrated in the test setup in Figure 3. As a result, the reaction force measured through the load cell corresponds to the blanking force on the specimen. The load displacement responses of the tests are plotted in Figure 7b. The abscissa which indicates the global displacement is measured by DIC as the vertical component of relative displacement between point ⓐ and ⓑ as illustrated by Figure 7a. These two points locate in the middle section of the thickness direction and are symmetric to the middle plane of the tool gap,

which is marked by the red dashed line in the figure. They served as the two branches of the virtual global extensometer in the current study. The initial gauge length is 1.5mm, which is sufficiently large that both tracing points are outside the tool gap so that their relative vertical displacement closely represents the blanking displacement. It is observed from Figure 7b that with the increase of die clearance, blanking displacement before total separation increases while the peak blanking load decreases. Also, the an abrupt fracture happened quickly after the blanking force peaked during the test. The load displacement curves dropped sharply at the end.

In addition, the relative vertical displacement between another set of tracing points labeled as ⓒ and ⓓ with initial gauge length of 0.15mm was extracted by DIC method and plotted in Figure 7c. These two tracing points locates inside the tool gap and will be addressed as local extensometer afterwards. Due to their small initial distance, they provide information that corresponds to deformation localization. As illustrated in Figure 7c, at large die clearance, the strain localizes slower than in smaller die clearance, which is because the deformation is spanned over a larger tool gap.

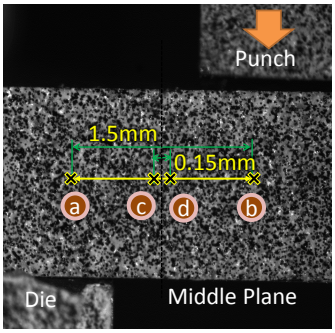

(a)

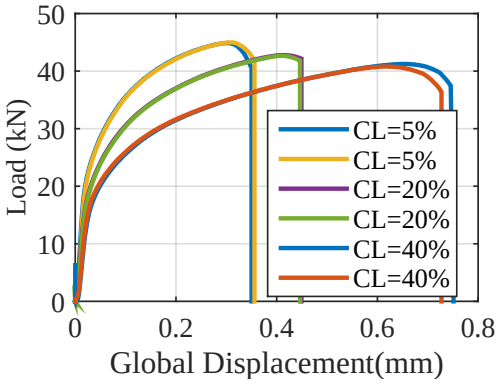

(b)

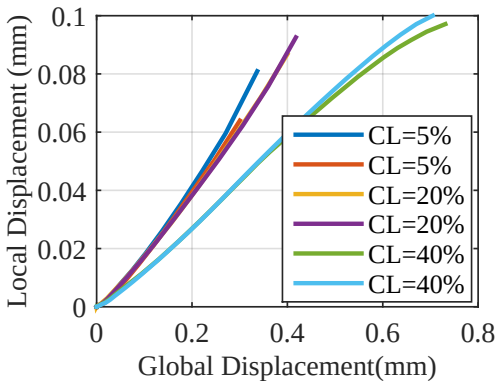

(c)

Fig. 7: Load displacement response and the evolution of the local displacement of blanking tests with different die clearances. There are two repeats of each die clearance.

3.3 Edge profile and surface quality observation

The blanked specimens were polished after test and the edge profiles resulting from different die clearances are illustrated in Figure 8. At all die clearances, the blanked edge showed clearly the geometry features of roll over, burnished zone and fracture zone, as conceptually illustrated in Figure 1a. At small die clearances of 5% and 20% there was no burr formed, while at die clearance of 40% a clear burr was formed.

The new edge surface created by the blanking process was observed under a scanning electron microscope (SEM) and the results corresponding to die clearance of CL=20% are illustrated in Figure 9. The blanked surface consists of two distinct regions: burnished zone and rupture zone. The burnished zone featured a shinning surface which was due to the high compression force between the punch head and the material as shown in Figure 9b. Additional results from interrupted tests in the following section revealed that the burnished zone was formed purely by plastic flow of the material. There was no crack formation or propagation in this region, as observed in Figure 10b. Rupture zone, however, was where crack initiated and propagated during the blanking process. Therefore, a rough surface is produced by material splitting. Right beneath the burnished zone, the material undergoes a combined loading of shear and tension, as observed in Figure 6. Therefore, the fracture surface features small dents as well as boundaries from shear rupture as indicated by Figure 9c. In the middle of the thickness direction, the deformation is dominated by shear and the fracture surface mainly have the sheared rupture boundaries without obvious dimples (Figure 9d).

(a)

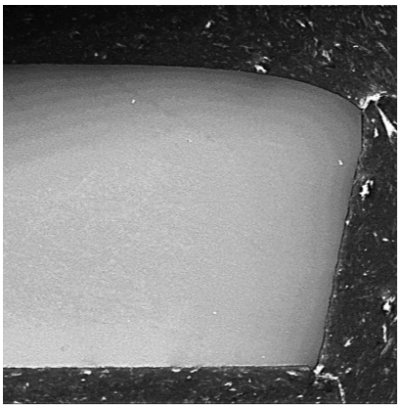

(b)

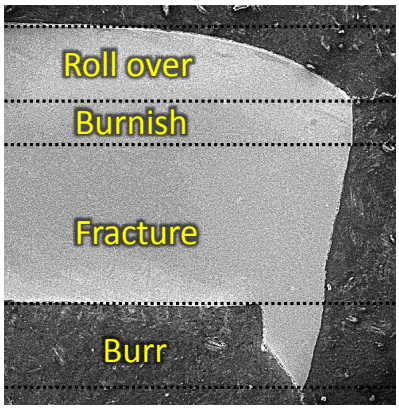

(c)

Fig. 8: Blanked edge profile of different die clearance: (a) 5%, (b) 20% and (c) 40%.

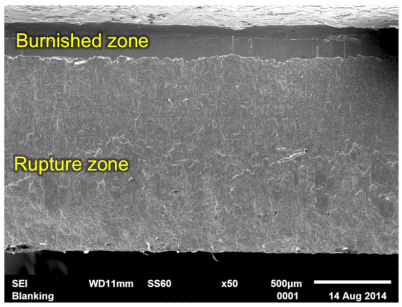

(a)

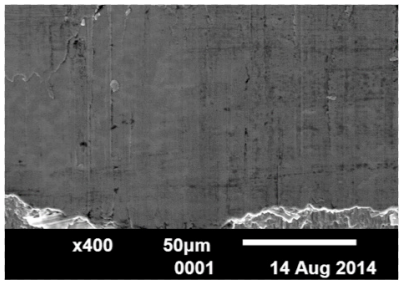

(b)

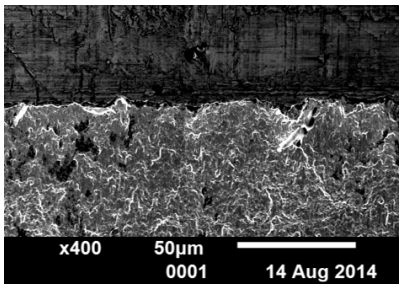

(c)

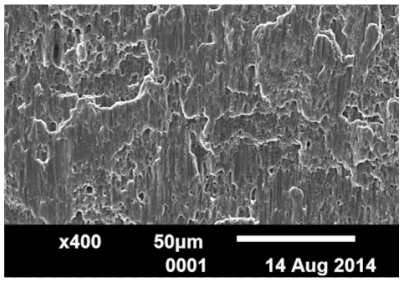

(d)

Fig. 9: New surface created by blanking under SEM observation, CL=20%. (a) The whole banked edge surface, (b) burnished zone, (c) transition zone at the border of burnished zone and rupture zone (d) shear zone in the middle of the thickness direction.

3.4 Interrupted test

Due to the abrupt fracture of the specimen during blanking, it was hard to observe the crack formation and propagation process by DIC. Interrupted tests were performed to clarify this issue. The tests were interrupted at different load level before maximum load or right after load peaks at three different stages (Fig.10) and two repeats were carried out for each stage. It was found that before blanking force peaks, there was only plastic deformation and no crack was formed (Figure 10a-b). In Figure 10b which illustrates a test interrupted before

load peaks, the burnished zone is clearly demonstrated while the punch head penetrated into the specimen in the zoomed-in view. A severe roll over happened to the right of the burnish surface, but no crack was formed at this stage.

After the blanking force peaks, a crack (or cracks) is formed and propagates quickly until a full separation of the specimen. Tests interrupted immediately after the load peaks showed that during blanking with a relatively small die clearance (5%) there were two cracks formed both at the punch side and the die side, as illustrated by Figure 10c. However during blanking with a large die clearance, only one crack was formed from the punch head side (Figure 11) while the second crack from the die side is absent. As a result, the material inside the tool gap stayed with the test piece, deformed around the die to create the burr feature shown in Figure 8c. This observation explains the mechanism of burr formation.

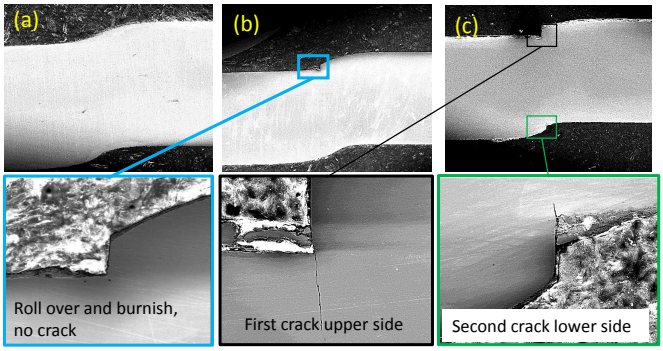

Fig. 10: Interrupted test results, crack formation and propagation sequence at die clearance of 5%.

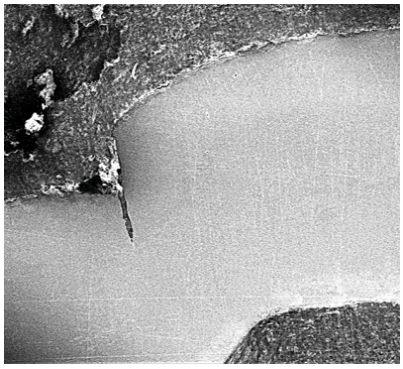

Fig. 11: Only one crack is formed during blanking with large die clearance of CL=40%.

3.5 Limitation of the test

The main limitation of the current plane-strain blanking test lies in that cameras used for DIC measurement can only observe the free surface of the specimen, where the material is not under pure plane-strain loading condition as it is at the cross sections inside the specimen. Materials at the free surface are allowed to deform in the out-of-plane direction, especially in the region close to the tool tip where the tool exerts a high compression on the material. As a result, although the burnishing process which features the penetration of the punch head (or the die) into the specimen was clearly observed from the interrupted tests(Figure 10b), it was not accurately captured by the DIC measurement on the side surface. As shown by Figure 5c, no tool penetration was observed. It was because materials close to the punch head tip moved in the out-of-plane direction and wrapped around the punch head. A closer look on the blanked surface under SEM (Figure 12) revealed more details about the difference between free edge surface and the inner cross section.

Figure 12a shows the newly blanked surface of a specimen. The right hand side of the specimen in the figure corresponds to the free surface observed by the microscope during the test. As shown in the figure, the burnished zone, which is the upper shining band on the surface, ended before it reached the free surface. In other words, burnishing process did not happen there. After interrupted test, when polishing specimen only slightly, the specimen shows a smooth cross section as illustrated in Figure 12c. This cross section is very similar to the free surface observed by the DIC. However, when further polishing the same specimen by another 0.3mm to reach the inner side, the cross-section of the specimen shows an obvious burnished region by the sharp turns, as demonstrated in Figure 12b. Note that the cross-section positions marked in Figure 12a are only conceptual and do not correspond to the exact location of the cross section in the following figures. Figure 12b-c were taken from the same specimen of a interrupted test, while Figure 12a was taken from a common blanking test.

4 FE Simulation

4.1 Modeling

Previous work by the authors Wang et al (2014) showed that the in-plane plasticity and fracture behavior of the current DP780 material can be accurately captured by the modeling framework featuring (a) Hill 48 yield function, (b) isotropic hardening, (c) associated flow rule,

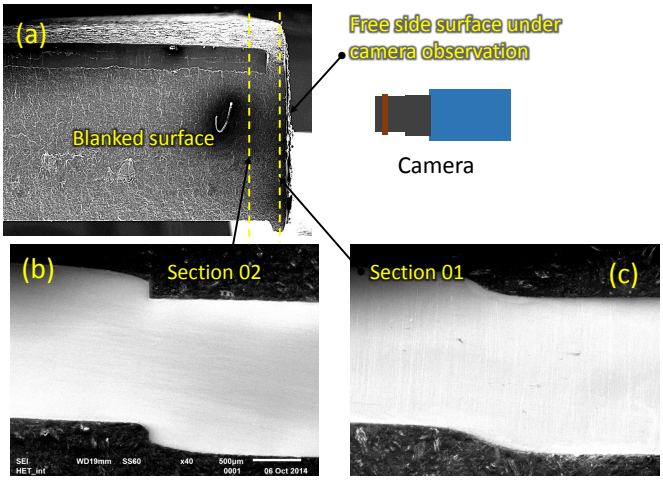

Fig. 12: Free side surface observed by the camera is different from inner cross section of the specimen which undergoes plane-strain loading condition.

and (d) the uncoupled MMC fracture model. As a starting point, the same modeling framework was continued in the current study. The Hill 48 yield function reads:

$$f(\boldsymbol{\sigma}) = \sqrt{F(\sigma_y-\sigma_z)^2 + G(\sigma_z-\sigma_x)^2 + H(\sigma_x-\sigma_y)^2 + 2L\tau_{yz}^2 + 2M\tau_{zx}^2 + 2N\tau_{xy}^2} \tag{1}$$

where, F, G, H, L, M, N are the anisotropic parameters and listed in Table 1 which were taken from the earlier publication Wang et al (2014).

The strain hardening behavior of the material was measured from dog-bone specimen tension test until localized necking happens and fitted by both Swift law (Eq. 2) and Voce form (Eq. 3). An optimized extrapolation of strain hardening behavior was then obtained by introducing a weighted combination α between these two hardening law (Eq. 4), which was tuned so that the post-necking load displacement behavior of the notched specimen tension test was accurately predicted by FE simulation.

$$Y_{\text{Swift}}(\bar{\varepsilon}^p) = A \cdot (\bar{\varepsilon}^p + \varepsilon_0)^n \tag{2}$$

$$Y_{\text{Voce}}(\bar{\varepsilon}^p) = Y_s - (Y_s - Y_0)\exp\left(-\frac{H_0}{Y_s}\bar{\varepsilon}^p\right) \tag{3}$$

$$Y(\bar{\epsilon}^p) = \alpha\, Y_{\text{Swift}}(\bar{\epsilon}^p) + (1-\alpha) Y_{\text{Voce}}(\bar{\epsilon}^p) \tag{4}$$

Fracture of the material was modeled by an uncoupled framework utilizing a damage accumulation formulation of:

$$D = \int_0^{\bar{\epsilon}_p} \frac{d\bar{\epsilon}_p}{\hat{\varepsilon}_f(\eta,\bar{\theta})} \tag{5}$$

where D is the damage indicator with $D = 0$ denotes the virgin state of the material without and damage and when $D = 1$ the material fails.

The recently formulated modified Mohr-Coulomb Model (MMC) by Bai and Wierzbicki (2010) was applied to define the fracture locus $\hat{\varepsilon}_f(\eta,\bar{\theta})$:

$$\hat{\varepsilon}_f = \left\{\frac{A}{c_2}\left[c_3 + \frac{\sqrt{3}}{2-\sqrt{3}}(1-c_3)\left(\sec\left(\frac{\bar{\theta}\pi}{6}\right)-1\right)\right]\right.\left[\sqrt{\frac{1+c_1^2}{3}}\cos\left(\frac{\bar{\theta}}{6}\right.\right. \tag{6}$$

where c_1, c_2 and c_3 are the three material parameters associated with the model that need to be calibrated.

Results of the material calibration were reported in Wang et al (2014, under review). The material parameters listed in Table 2 were reused in the current study. The models were implemented through a user material subroutine VUMAT in Abaqus.

A plane-strain finite element model (CPE4R plane strain element of the Abaqus element library) was implemented first with ideally rigid boundary conditions. As shown in Figure 13, the model features a very fine mesh with size of 0.01mm in the vicinity of the tool gap, which is required to accurately capture the high strain gradient associated with the blanking process. For simplicity only half of the specimen was modeled with a symmetric boundary condition applied to the specimen at the plane of symmetry. The blanking tools were modeled as analytical rigid body. Both the die and die holder were fixed rigidly while the punch head was allowed to move only in the vertical direction to cut the specimen. A kinematic method of surface to surface contact in Abaqus was applied between the blanking tools and the specimen. A friction coefficient of 0.2 was assigned which was measured from a friction test.

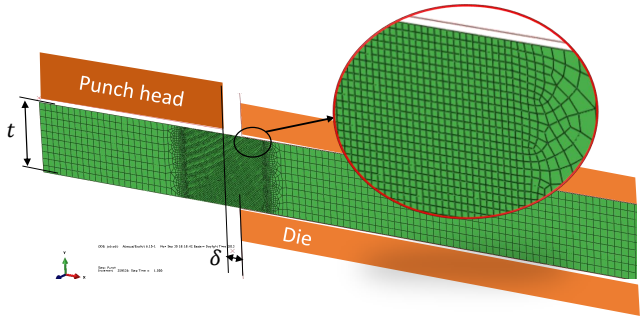

Fig. 13: 2D plane-strain model for blanking simulation.

Table 1: Anisotropy parameters of DP780: Lankford ratio and Hill 48 model parameter(Wang et al, 2014).

r_0	r_{45}	r_{90}	F	G	H	L	M	N
0.7031	0.9434	0.6237	0.6619	0.5872	0.4128	1.5	1.5	1.8029

Table 2: Strain hardening and MMC fracture model parameters of DP780.

A[MPa]	$\bar{\varepsilon}_0$[-]	n[-]	Y_s[MPa]	Y_0[MPa]	H_0[MPa]	α[-]	c_1[-]	c_2[MPa]	c_3[-]
1460	0.0024	0.194	1020	508	19310	0.7	0.107	758	0.972

4.2 Preliminary simulation results

Load displacement response as well as the local virtual extensometer history were extracted from the simulation to compare with the tests results and plotted in Figure 14a-b. The die clearance was 20%. Under the stated condition the FE model was more rigid compared with the test results. The load displacement response predicted overshoot by a large amount the test result. In terms of local extensometer, the localization happened earlier in FE simulation than that measured from tests. The final edge profile predicted by simulation was compared with tests result in Figure 14c. The lower side of the punch head corresponds to the ending point of the burnished zone. It was clear that the size of the roll over region, burnished zone were both underestimated while the fracture zone was overestimated. The preliminary model failed to give a good prediction in terms of quantitative correlation with the blanking test.

There are two reasons for the above discrepancies:

1. The plasticity and fracture model were calibrated through in-plane tests while the blanking process mainly involves material behavior in the out-of-plane direction. The material behavior of the out-of-plane direction might be much different from in-plane direction.
2. The mismatch in boundary conditions. The ideally rigid blanking tool as well as the rigid constraints introduced during the simulation do not agree with the actual boundary conditions in tests.

Those two aspects will be addressed in the following sections and improvements will be made to the model.

4.3 Out-of-plane compression test and non-associated flow rule

Due to the small thickness of 1.6mm of the steel sheet, tests in the thickness direction is quite challenging and only limited test options are available such as compression test and shearing test. The blanking test itself can serve an out-of-plane test that can be used to calibrate of the material model. However, the model calibrated this way may lose generality because it is incorrect to calibrate and validate a model from the same test. Therefore, an out-of-plane compression test using multiple layer of disk specimen was used in the current study to determine the plasticity behavior of the material in the thickness direction. The test procedure was illustrated in Figure 15a. Five layers of disk specimens with initial diameter of 10mm were stacked together and compressed under the MTS load frame. Teflon film as well as high pressure lubrication grease was put between the specimen and the test machine to reduce the friction. DIC method was used to measure the specimen deformation while the force was recorded directly by the load cell of the test machine. The true stress strain curve in the thickness direction was then obtained and plotted in Figure 15c, and compared with that obtained from the in-plane dog-bone tension test in 0 degree to rolling direction. The curve reached a plastic strain as high as 0.4 without fracture, compared with only 0.14 of the in-plane tension test. Also it almost perfectly overlaps with the in-plane stress strain curve of the rolling direction, indicating no obvious anisotropy in the strain hardening behavior.

According to the modeling framework outlined in Section 4.1, the strain hardening behavior of the out-of-plane direction can be obtained from that in the rolling direction through:

$$\sigma_z = \sqrt{\frac{G+H}{G+F}} \cdot \sigma_0 \tag{7}$$

where F, G and H are the parameters of the Hill 48 model, σ_0 is the flow strength of the in-plane rolling direction while σ_z denotes the yield stress in the thickness direction. Following the associated flow rule (AFR), the parameters were calibrated from Lankford ratios and listed in Table 1. The stress strain curve obtained following AFR was plotted as the red dotted curve in

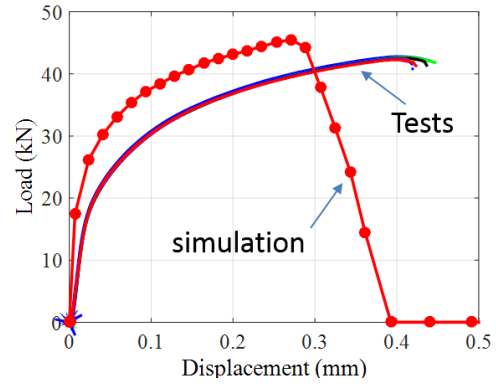

(a)

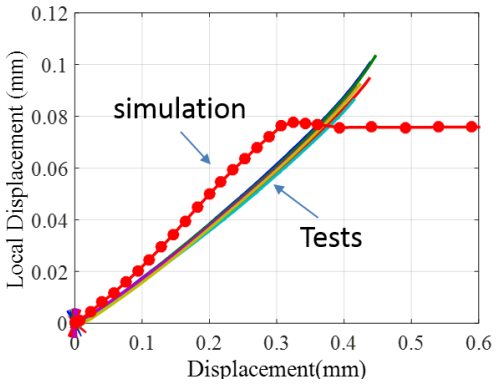

(b)

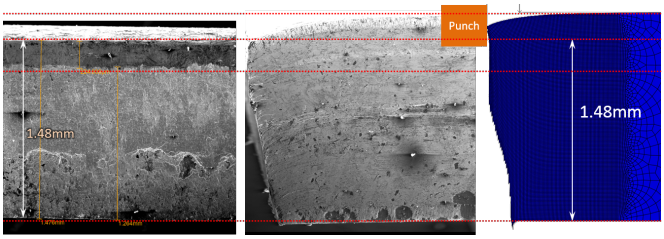

(c)

Fig. 14: Blanking simulation results of the preliminary FE model in comparison with test results. (a) load displacement response, (b) local extensometer history, (c) edge geometry comparison.

Figure 15c. There was a big discrepancy between the test data and the AFR curve, suggesting the AFR assumption does not apply in the current situation for the material behavior of out-of-plane direction. In view of this, a non-associated flow rule (nAFR) was assumed in the following study. Following the work by Mohr et al (2010), a yield function as well as a flow potential function were defined separately in Eq.8 and Eq.10. The yield function controls shape of the material yield surface, while the flow potential function determines the direction of the plastic strain increment.

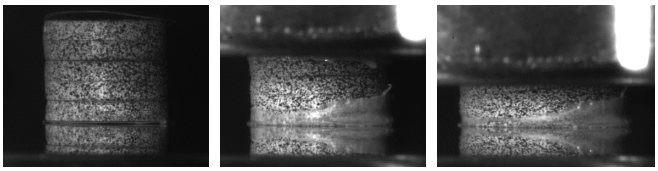

(a)

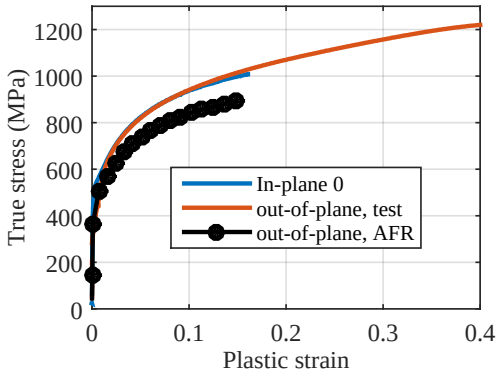

(b)

Fig. 15: Out-of-plane compression test and the stress strain curve in thickness direction.

The yield condition reads:

$$f(\boldsymbol{\sigma}, Y) = \bar{\sigma} - Y \tag{8}$$

where Y denotes the yield strength which is a function of the equivalent plastic strain, while $\bar{\sigma}$ is the equivalent stress that takes the following form:

$$\bar{\sigma} = \sqrt{\boldsymbol{\sigma} \cdot \underline{\underline{\mathbf{P}}} \boldsymbol{\sigma}} \tag{9}$$

The flow potential reads:

$$g(\boldsymbol{\sigma}) = \sqrt{\boldsymbol{\sigma} \cdot \underline{\underline{\mathbf{G}}} \boldsymbol{\sigma}} \tag{10}$$

The $\boldsymbol{\sigma}$ in both Eq.9 and Eq.10 denotes the Voigt notation of Cauchy stress tensor:

$$\boldsymbol{\sigma} = [\sigma_{xx} \quad \sigma_{yy} \quad \sigma_{zz} \quad \sigma_{yz} \quad \sigma_{zx} \quad \sigma_{xy}]^\top \tag{11}$$

Instead of using the normal direction of the yield function to determine the plastic flow direction, the material flow is governed by the flow potential function as:

$$\mathrm{d}\boldsymbol{\varepsilon}^p = \frac{\partial g}{\partial \boldsymbol{\sigma}} \cdot \mathrm{d}\gamma \tag{12}$$

where $\mathrm{d}\gamma \geq 0$ is a scalar plastic strain multiplier and $\mathrm{d}\boldsymbol{\varepsilon}^p$ is the Voigt notation of incremental plastic strain tensor that is work conjugated to the Voigt notation of Cauchy stress tensor $\boldsymbol{\sigma}$:

$$\mathrm{d}\boldsymbol{\varepsilon}^p = [\mathrm{d}\varepsilon^p_{xx} \quad \mathrm{d}\varepsilon^p_{yy} \quad \mathrm{d}\varepsilon^p_{zz} \quad 2\mathrm{d}\varepsilon^p_{yz} \quad 2\mathrm{d}\varepsilon^p_{zx} \quad 2\mathrm{d}\varepsilon^p_{xy}]^\top$$

(13)

Both the yield function and the flow potential function still take the quadratic Hill 48 form by introducing the special form of coefficient matrix $\underline{\underline{\mathbf{P}}}$ and $\underline{\underline{\mathbf{G}}}$ as shown in Eq.14 and Eq.15.

$$\underline{\underline{\mathbf{P}}} = \begin{bmatrix} G+H & -H & -G & 0 & 0 & 0 \\ -H & F+H & -F & 0 & 0 & 0 \\ -G & -F & F+G & 0 & 0 & 0 \\ 0 & 0 & 0 & 2L & 0 & 0 \\ 0 & 0 & 0 & 0 & 2M & 0 \\ 0 & 0 & 0 & 0 & 0 & 2N \end{bmatrix} \tag{14}$$

$$\underline{\underline{\mathbf{G}}} = \begin{bmatrix} G^P+H^P & -H^P & -G^P & 0 & 0 & 0 \\ -H^P & F^P+H^P & -F^P & 0 & 0 & 0 \\ -G^P & -F^P & F^P+G^P & 0 & 0 & 0 \\ 0 & 0 & 0 & 2L^P & 0 & 0 \\ 0 & 0 & 0 & 0 & 2M^P & 0 \\ 0 & 0 & 0 & 0 & 0 & 2N^P \end{bmatrix} \tag{15}$$

In the special case of $\underline{\underline{\mathbf{P}}} = \underline{\underline{\mathbf{G}}}$, the model is reduced to AFR. In nAFR however, the flow potential coefficient of $\underline{\underline{\mathbf{G}}}$ is taken as different from yield function coefficient $\underline{\underline{\mathbf{P}}}$.

According to Figure 15c the strain hardening curve in the thickness direction overlapped perfectly with the one of the in-plane rolling direction. Therefore a simplified von Mises yield function was assumed for the following study with the yield function parameters listed in Table 3. The plastic flow?however, were significantly anisotropic which is indicated by the Lankford ratios substantially deviates from unity as listed in Table 1. Therefore, the Hill 48 flow potential function was implemented. Parameters of the flow potential function were calibrated from Lankford ratios and therefore remained identical to those in Table 1.

Table 3: Parameters of the yield function coefficient $\underline{\underline{\mathbf{P}}}$ that reduces the model to von Mises yield condition.

F	G	H	L	M	N
0.5	0.5	0.5	1.5	1.5	1.5

In terms of the fracture behavior, it was still assumed that the material behaves the same in out-of-plane direction as in-plane direction.

4.4 Boundary condition improvement

Besides the plasticity model, boundary conditions of the model need to be improved to ensure a better agreement with the actual tests. With DIC measurement, the blanking tools were also under observation during the test besides the specimen. Therefore, deformation as well as displacement information in the tools could be extracted from the test data. As illustrated in Figure 16a, the horizontal displacement (denoted as U in the figure) as well as vertical displacements (denoted as V) of both the punch head and the die were obtained by DIC for a blanking test with die clearance of 20%. It was obvious that compared with the punch displacement, there was also a substantial horizontal displacement in the die. This displacement was caused by the elastic deformation of the die as well as the test platform. At the end of the test, the horizontal displacement of the punch head is about 0.95mm while that of the die is 0.28mm. Besides the horizontal movement, there was also vertical displacement in both die and punch head. The vertical displacement was relatively small compared with the horizontal component. However, it was significant when compared with the tool gap. The relative vertical displacement between the punch and the die caused the die clearance to reduce from the original 0.33mm to the final 0.28mm as shown in Figure 16b.

Besides the global displacements, there was also local elastic deformation in the punch, especially close to the tool tip. As illustrated in Figure 17, in-plane strain components were extracted from the DIC data at two spots on the punched head. Spot (1) locates close to the tool tip which is about 0.05mm away while spot (2) locates about 0.15mm away. Figure 17b demonstrates that both shear strain ε_{xy} and horizontal compressive strain ε_{xx} at location (1) saw a sharp turn close to the end, denoting yielding happened at the tool tip. Therefore, it is important to treat the tool as deformable instead of ideally rigid in the simulation.

Tool edge radii which corresponds to the tool sharpness has been proven to be an critical parameter during the blanking process(Golovashchenko, 2006). Assuming an ideally sharp tool edge is dangerous and may even cause numerical error. It is equally imprudent to choose an arbitrary value while having no measurement on the radii. However, it is hard to measure the sharp tool radii directly. In the current study, an indirect method was used to obtain this information. It was found that the blanked specimen will plastically deform to bend around the tool tip. As a result, the tool tip profile will be imprinted into the blanked specimen. As shown in Figure 18, the smooth transition between the burr fea-

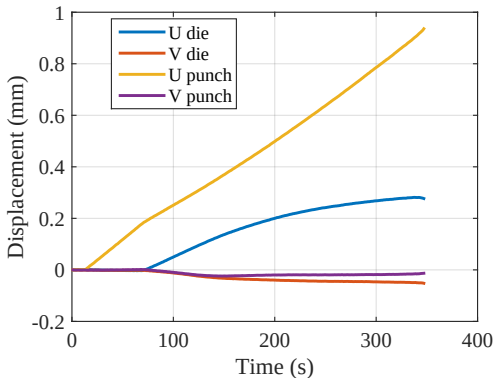

(a)

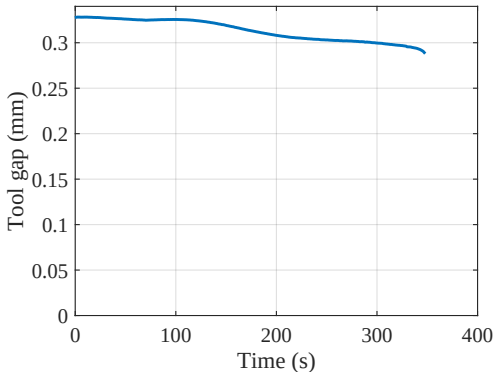

(b)

Fig. 16: (a) displacement of the blanking tools during the test. (b) Tool gap change due to the relative movement between die and punch during the test.

ture and the specimen denotes the tool radii, which was $r = 47\mu$m as measured by SEM.

As illustrated in Figure 19, in the updated model, the blanking tool was modeled as a deformable with a tool radii of 0.05mm. The material heat treated of the tool was elastic plastic with yield strength of 2200MPa. The die was still fixed firmly in the updated model. However, in addition to blanking displacement Δ_V, an horizontal displacement Δ_H of the punch head was introduced and the maximum displacement value was obtained by DIC from the corresponding test data. Considering the blank holder was tightened by only two screws and was not capable of introducing ideally rigid constraint, a small gap of 0.1mm was introduced between the blanking holder and the test piece. This change was relatively arbitrary compared with other quantified improvements but still provides a reasonable approximation of the real situation.

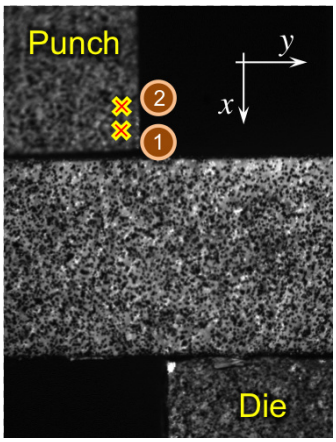

(a)

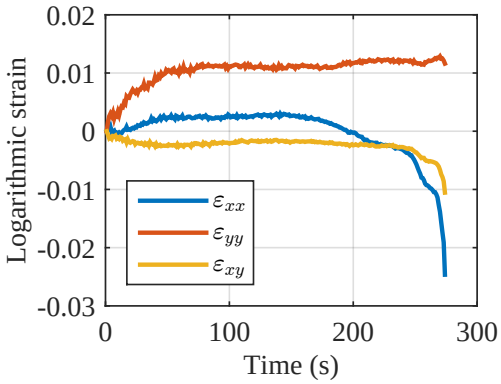

(b)

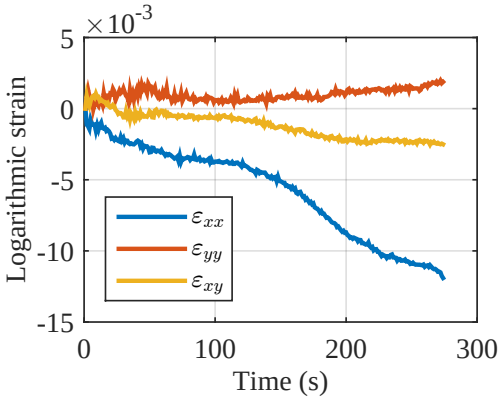

(c)

Fig. 17: Deformation in the blanking tools during the test. (a) Locations where the strain information was extracted using DIC, (b) deformation history of location 1, (c) deformation history of location 2.

4.5 FE simulation results

The improved FE model yield a very accurate prediction of the blanking process and shows a close correlation with the test results. The load displacement re-

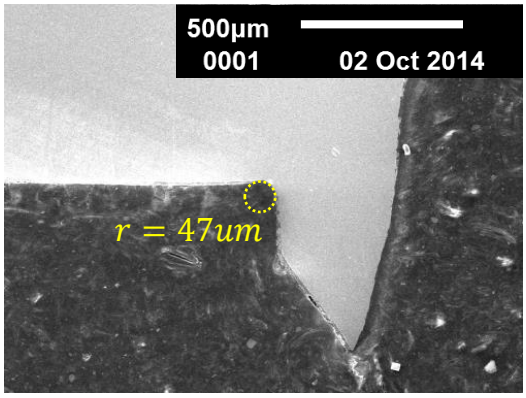

Fig. 18: Blanking tool radii measured from the edge profile after test.

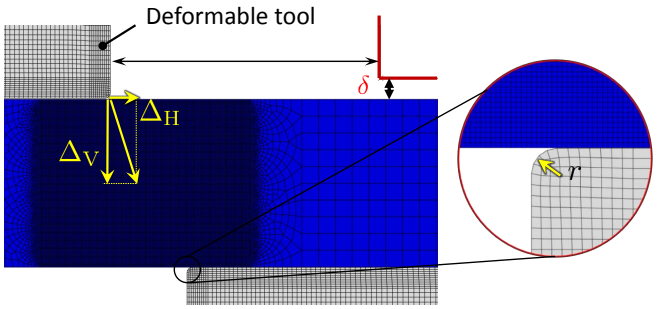

Fig. 19: Improvements in boundary conditions of simulation to stay more consistent with the actual blanking tests.

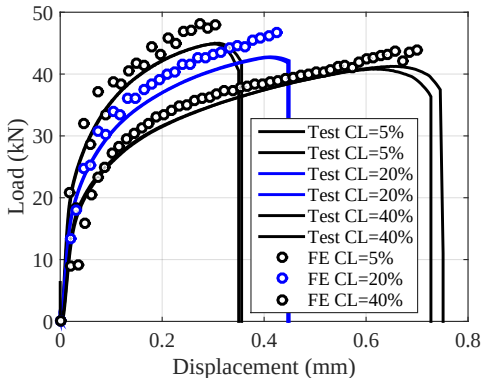

(a)

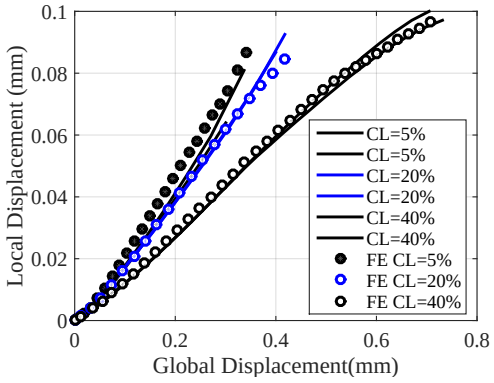

(b)

Fig. 20: (a) load displacement response and (b) local extensometer history from blanking simulation with the improved boundary conditions. Simulation compared with test results.

sponse as well as local extensometer history were compared with test results in Figure 20. The dotted curves denote the simulation results while solid curves correspond to test results. The different die clearances are distinguished by different colors. It is clear that the new model can accurately predict the global response of load displacement history during the blanking test, as well as the local deformation gradient in terms of the local extensometer.

The predicted crack initiation and propagation sequence is summarized in Figure 21 for blanking with die clearance of 5%. The process of plastic strain localization, crack formation and propagation is predicted in close correlation with test results in Figure 10. The crack formation and propagation is also predicted by the model. There are two cracks initiated, one beneath the punch head and another one close to the die side. The two cracks propagate in thickness direction and meet inside the specimen until the total separation. The prediction closely correlates with the interrupted test results.

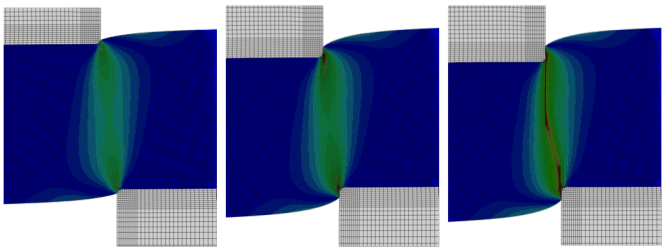

Fig. 21: Crack formation and propagation sequence during blanking with die clearance of 5% predicted by FE simulation, which has a close correlation with test results in Figure 10. Contour plots are the simulation results and the color code is damage indicator.

During blanking with large die clearance of 40% there is only one crack formed as predicted in Figure 22, which also agrees with the test result in Figure 11.

In terms of fracture prediction, the blanked edge profile in FE simulation is compared with test result in Figure 23. The geometry features of roll over, burnish

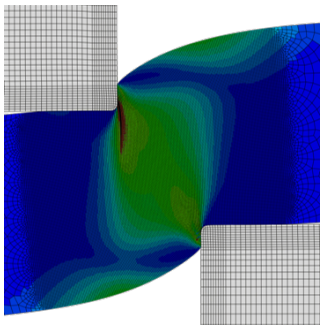

Fig. 22: FE prediction showed that only one crack is formed during blanking with large die clearance of 40%, which agrees with the test result in Figure 11. The contour illustrates damage indicator.

and fracture zone are all accurately predicted quantitatively. The burr feature was also predicted in large die clearance of 40%, with an accurate capturing of the burr hight. However, there was one feature that was not accurately predicted, which was the fracture angle as illustrated in Figure 23. Prediction of fracture angle is a complicated issue that relates to the crack propagation. In the current study, an element deletion method was employed to model material fracture and crack propagation. The crack propagation path depends on many factors including mesh size, mesh orientation, material post softening after reaching crack criterion, and others, which is not pursued in detail within the current study.

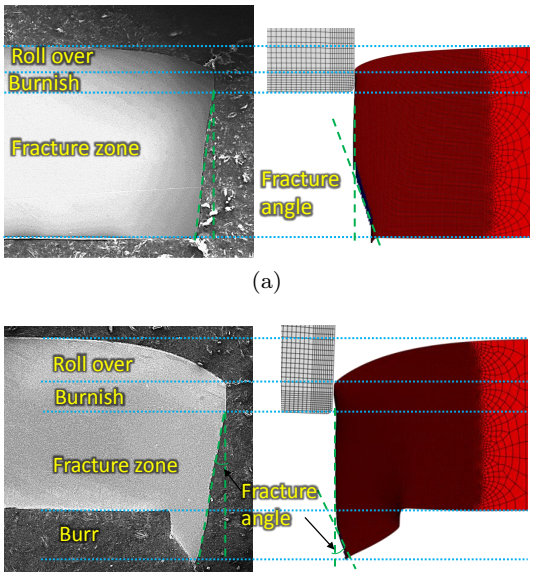

Fig. 23: Predicted edge profile shows a quantitative correlation with the test data. (a) CL=5%, (b) CL=40%.

5 Conclusion

A plane-strain blanking test was successfully carried out on a DP780 steel sheet with a real time DIC deformation measurement on the blanking surface. The challenges of performing such a test caused by the small gauge section (less than 2x2mm in area) as well as the high load level (around 50kN) were solved by a newly developed test apparatus with high rigidity as well as the DIC measurement system using an in-situ microscope that promises enough magnification. Detail information about whole field deformation was extracted on the blanked surface with high resolution. It is the first time that the specimen deformation during a sheet blanking process is reported with such a high accuracy. The DIC measurement also provided the authors experimental data that was utilized to verify the following finite element simulation. Interrupted tests were carried out to study the abrupt crack initiation and propagation during a blanking test. Results showed that two cracks were formed when blanking with a small die clearance, while only one crack was formed under the punch head and propagate throughout the thickness when blanking with a large die clearance. The burr feature was formed at large die clearance due to only one crack was initiated.

In the Finite Element simulation side, one additional tests of upsetting in the thickness direction was added to calibrate the plasticity model. The study indicated that the DP780 material possess a strong anisotropy in terms of plastic flow, while the hardening behavior in the thickness direction is almost identical to that of the in-plane rolling direction. This calls for the introduction of the non-associated flow rule in the model. The final modeling frame work consisted of the modified Mohr-Coulomb fracture model and a plasticity model featuring (a) von Mises yield condition, (b) Hill 48 flow potential function, (c) non-associated flow rule and (d) isotropic hardening. Fracture parameters calibrated from in-plane tests were used to simulate the material behavior in the out-of-plane direction with success. No additional fracture calibration test is required. With accurate boundary conditions measured from the tests, the model yielded an accurate prediction of the blanking process.

Acknowledgments

The authors want to thank Dr. Lars Greve for valuable discussions. Thanks are also due to Altair for providing free educational Hypermesh license which were used to prepare part of the finite element models used in the

current study. We want to acknowledge the MIT Industrial Fracture Consortium for the funding support of the current study.

References

Bai Y, Wierzbicki T (2010) Application of extended mohr–coulomb criterion to ductile fracture. International Journal of Fracture 161:1–20, URL http://dx.doi.org/10.1007/s10704-009-9422-8, 10.1007/s10704-009-9422-8

Cockcroft MG, Latham DJ (1966) A simple criterion of fracture for ductile metals

Dalloz A, Besson J, Gourgues-Lorenzon T AFand Sturel, Pineau A (2009) Effect of shear cutting on ductility of a dual phase steel. Engineering Fracture Mechanics 76(10):1411–1424

Dykeman J, Malcolm S, Yan B, Chintamani J, Huang G, Ramisetti N, Zhu H (2011) Characterization of edge fracture in various types of advanced high strength steel. Tech. rep., SAE Technical Paper

Goijaerts A, Stegeman Y, Govaert L, Brokken D, Brekelmans W, Baaijens F (2000) Can a new experimental and numerical study improve metal blanking? Journal of Materials Processing Technology 103(1):44–50

Golovashchenko SF (2006) A study on trimming of aluminum autobody sheet and development of a new robust process eliminating burrs and slivers. International journal of mechanical sciences 48(12):1384–1400

Golovashchenko SF (2008) Quality of trimming and its effect on stretch flanging of automotive panels. Journal of Materials Engineering and Performance 17(3):316–325

Golovashchenko SF, Ilinich AM (2005) Trimming of advanced high strength steels. In: ASME 2005 International Mechanical Engineering Congress and Exposition, American Society of Mechanical Engineers, pp 279–286

Hambli R, Reszka M (2002) Fracture criteria identification using an inverse technique method and blanking experiment. International journal of mechanical sciences 44(7):1349–1361

Hu X, Choi KS, Sun X, Golovashchenko SF (2014) Edge fracture prediction of traditional and advanced trimming processes for aa6111-t4 sheets. Journal of Manufacturing Science and Engineering 136(2):021,016

Konieczny A, Henderson T (2007) On formability limitations in stamping involving sheared edge stretching. Tech. Rep. 2007-01-0340, SAE International, Warrendale, PA, URL http://digitallibrary.sae.org.libproxy.mit.edu/content/2007-01-0340

Li M (2000a) An experimental investigation on cut surface and burr in trimming aluminum autobody sheet. International Journal of Mechanical Sciences 42(5):889–906

Li M (2000b) Micromechanisms of deformation and fracture in shearing aluminum alloy sheet. International journal of mechanical sciences 42(5):907–923

Mohr D, Dunand M, Kim KH (2010) Evaluation of associated and non-associated quadratic plasticity models for advanced high strength steel sheets under multi-axial loading. International Journal of Plasticity 26(7):939–956, 626NE Times Cited:17 Cited References Count:60

Rice JR, Tracey DM (1969) On the ductile enlargement of voids in triaxial stress fields. Journal of the Mechanics and Physics of Solids 17(3):201–217

Samuel M (1998) Fem simulations and experimental analysis of parameters of influence in the blanking process. Journal of Materials Processing Technology 84(1):97–106

Shih HC, Chiriac C, Shi MF (2010) The effects of ahss shear edge conditions on edge fracture. In: ASME 2010 International Manufacturing Science and Engineering Conference

Stegeman Y, Goijaerts A, Brokken D, Brekelmans W, Govaert L, Baaijens F (1999) An experimental and numerical study of a planar blanking process. Journal of Materials Processing Technology 87(1):266–276

Thipprakmas S, Jin M, Tomokazu K, Katsuhiro Y, Murakawa M (2008) Prediction of fineblanked surface characteristics using the finite element method (fem). Journal of Materials Processing Technology 198(1):391–398

Wang K, Luo M, Wierzbicki T (2014) Experiments and modeling of edge fracture for an ahss sheet. International Journal of Fracture pp 1–24, DOI 10.1007/s10704-014-9937-5, URL http://dx.doi.org/10.1007/s10704-014-9937-5

Wang K, Greve L, Wierzbicki T (under review) Fe simulation of edge fracture considering pre-damage from blanking process. IJSS

Zhou Q, Wierzbicki T (1996) A tension zone model of blanking and tearing of ductile metal plates. International journal of mechanical sciences 38(3):303–324